Linking snow microstructure to its macroscopic elastic stiffness tensor: A numerical homogenization method and its application to 3D images from X-ray tomography
– Supporting Information –

Antoine Wautier,[1,2,3] Christian Geindreau,[2,3] Frédéric Flin[1]

[1]Météo-France – CNRS, CNRM-GAME UMR 3589, CEN, F-38400 Saint Martin d'Hères, France
[2]Université Grenoble Alpes, 3SR, F-38000 Grenoble, France
[3]CNRS, 3SR, F-38000 Grenoble, France

Supporting Information for Wautier, A., C. Geindreau, and F. Flin (2015), Linking snow microstructure to its macroscopic elastic stiffness tensor: A numerical homogenization method and its application to 3-D images from X-ray tomography, *Geophys Res. Lett., 42, doi:10.1002/2015GL065227*

1 Numerical data

This section summarizes the data used in the titled paper. They concern 31 snow samples taken from the CEN database (see e.g. *Calonne et al.*, 2012). Table 1 focuses on the geometrical properties while Tables 2 and 3 correspond to the mechanical properties that were computed thanks to the homogenization procedure described in the article.
In Table 1, the snow types are designated according to the international classification (*Fierz et al.*, 2009). The correlation lengths (ℓ_1, ℓ_2, ℓ_3) were computed according to *Löwe et al.* (2013). In Table 2, the anisotropy indicators $A(E)$ and $A(G)$ are defined as in the eq. (6) of the titled paper:

$$A(E) = \frac{E_3}{(E_1 + E_2)/2}, \qquad A(G) = \frac{G_{12}}{(G_{23} + G_{13})/2}.$$

Sample name	Snow type	Dim (px)	Dim (mm)	Resolution (μm/px)	Snow density (kg/m^3)	Porosity	Correlation lengths (ℓ_1, ℓ_2, ℓ_3) (μm)
PP_102kg_512	PP	512	2.51	4.91	102.90	0.89	(57, 56, 55)
PP_113kg_600	PP	600	2.95	4.91	113.44	0.88	(65, 63, 61)
PP_123kg_600	PP	600	2.95	4.91	123.31	0.87	(64, 64, 65)
DF_157kg_512	DF	512	4.40	8.59	157.58	0.83	(101, 119, 72)
DF_147kg_512	DF	512	2.51	4.91	147.71	0.84	(91, 81, 83)
RG_172kg_600	RG	600	2.95	4.91	172.74	0.81	(92, 94, 97)
RG_192kg_600	RG	600	2.95	4.91	192.47	0.79	(103, 109, 103)
RG_198kg_600	RG	600	2.95	4.91	198.64	0.78	(115, 119, 112)
RG_256kg_512	RG	512	2.51	4.91	256.28	0.72	(113, 111, 110)
RG_280kg_512	RG	512	4.41	8.61	280.07	0.69	(127, 131, 86)
1A_350_30LC	RG	350	2.94	8.40	277.23	0.70	(95, 98, 91)
0A_261_30LC	RG	261	2.19	8.39	285.4	0.69	(70, 73, 66)
RG_315kg_512	RG	512	3.15	6.16	315.50	0.66	(115, 97, 115)
RG_1600	RG	600	4.46	7.43	330.13	0.64	(117, 111, 108)
RG_1600sup800	RG	600	4.46	7.43	337.68	0.63	(118, 119, 100)
RG_354kg_512	RG	512	3.15	6.16	354.51	0.61	(73, 76, 68)
RG_359kg_600	RG	600	3.69	6.15	359.84	0.61	(95, 94, 85)
RG_378kg_512	RG	512	4.38	8.55	378.96	0.59	(116, 115, 92)
RG_396kg_512	RG	512	3.12	6.10	396.07	0.57	(155, 147, 155)
RG_396.1kg_512	RG	512	3.15	6.16	396.13	0.57	(143, 139, 109)
RG_430kg_651	RG	651	5.61	8.61	430.59	0.53	(83, 82, 81)
2A_401_30LC	FC	401	3.36	8.37	280.11	0.69	(104, 109, 112)
3A_511_30LC	DH	511	4.29	8.40	278.00	0.70	(128, 133, 143)
4A_622_30LC	DH	622	5.22	8.40	314.24	0.66	(146, 147, 174)
5G_628_30LC	DH	628	6.06	9.66	292.88	0.68	(160, 160, 202)
7G_698_30LC	DH	698	6.74	9.66	316.77	0.65	(181, 182, 225)
MF_495kg_651	MF	651	5.60	8.61	495.11	0.46	(219, 226, 244)
MF_502kg_651	MF	651	5.59	8.59	502.60	0.45	(180, 189, 200)
MF_512kg_651	MF	651	5.59	8.59	512.89	0.44	(160, 162, 159)
MF_522kg_542	MF	542	5.42	10.00	522.31	0.43	(138, 134, 133)
MF_544kg_651	MF	651	5.60	8.61	544.08	0.41	(172, 168, 179)

Table 1: Geometrical properties.

Supporting Information for Wautier, A., C. Geindreau, and F. Flin (2015), Linking snow microstructure to its macroscopic elastic stiffness tensor: A numerical homogenization method and its application to 3-D images from X-ray tomography, *Geophys Res. Lett., 42, doi:10.1002/2015GL065227*

Sample name	Porosity	$A(E)$	$A(G)$	E_1/E_{ice}	E_2/E_{ice}	E_3/E_{ice}	G_{12}/G_{ice}	G_{13}/G_{ice}	G_{23}/G_{ice}
PP_102kg_512	0.89	0.86	1.21	5.48 E^{-3}	6.10 E^{-3}	4.98 E^{-3}	5.27 E^{-3}	4.37 E^{-3}	4.34 E^{-3}
PP_113kg_600	0.88	1.46	1.27	7.28 E^{-3}	7.58 E^{-3}	6.33 E^{-3}	6.82 E^{-3}	5.56 E^{-3}	5.15 E^{-3}
PP_123kg_600	0.87	0.99	0.96	6.93 E^{-3}	8.96 E^{-3}	7.87 E^{-3}	5.95 E^{-3}	5.51 E^{-3}	6.87 E^{-3}
DF_157kg_512	0.83	0.56	1.45	1.24 E^{-3}	1.36 E^{-3}	7.31 E^{-3}	1.14 E^{-2}	8.31 E^{-3}	7.42 E^{-3}
DF_147kg_512	0.84	1.03	0.95	1.45 E^{-2}	1.28 E^{-2}	1.40 E^{-2}	1.22 E^{-2}	1.39 E^{-2}	1.19 E^{-2}
RG_172kg_600	0.81	0.87	1.28	1.73 E^{-2}	1.65 E^{-2}	1.47 E^{-2}	1.59 E^{-2}	1.19 E^{-2}	1.30 E^{-2}
RG_192kg_600	0.79	0.99	1.06	2.03 E^{-2}	2.10 E^{-2}	2.03 E^{-2}	2.00 E^{-2}	1.71 E^{-2}	2.07 E^{-2}
RG_198kg_600	0.78	0.81	1.12	2.58 E^{-2}	2.42 E^{-2}	2.02 E^{-2}	2.26 E^{-2}	1.93 E^{-2}	2.10 E^{-2}
RG_256kg_512	0.72	0.90	1.10	5.22 E^{-2}	4.59 E^{-2}	4.40 E^{-2}	4.38 E^{-2}	4.37 E^{-2}	3.57 E^{-2}
RG_280kg_512	0.69	0.58	1.47	6.03 E^{-2}	5.55 E^{-2}	3.33 E^{-2}	5.76 E^{-2}	4.03 E^{-2}	3.77 E^{-2}
1A_350_30LC	0.70	1.20	0.95	3.54 E^{-2}	3.88 E^{-2}	4.46 E^{-2}	3.61 E^{-2}	3.70 E^{-2}	3.93 E^{-2}
0A_261_30LC	0.69	0.89	1.08	5.85 E^{-2}	5.20 E^{-2}	4.89 E^{-2}	5.40 E^{-2}	4.89 E^{-2}	5.10 E^{-2}
RG_315kg_512	0.66	1.10	0.91	7.17 E^{-2}	5.52 E^{-2}	6.97 E^{-2}	6.24 E^{-2}	7.42 E^{-2}	6.34 E^{-2}
RG_1600	0.64	0.94	1.03	6.06 E^{-2}	5.91 E^{-2}	5.62 E^{-2}	6.01 E^{-2}	5.70 E^{-2}	5.94 E^{-2}
RG_1600sup800	0.63	0.86	1.13	6.20 E^{-2}	6.85 E^{-2}	5.63 E^{-2}	6.83 E^{-2}	5.94 E^{-2}	6.19 E^{-2}
RG_354kg_512	0.61	0.94	1.02	8.35 E^{-2}	8.79 E^{-2}	8.10 E^{-2}	8.93 E^{-2}	8.53 E^{-2}	8.93 E^{-2}
RG_359kg_600	0.61	0.92	1.01	8.15 E^{-2}	8.05 E^{-2}	7.47 E^{-2}	8.09 E^{-2}	8.18 E^{-2}	7.89 E^{-2}
RG_378kg_512	0.59	0.73	1.23	1.10 E^{-1}	1.10 E^{-1}	8.02 E^{-2}	1.15 E^{-1}	9.39 E^{-2}	9.25 E^{-2}
RG_396kg_512	0.57	0.91	1.09	1.24 E^{-1}	1.17 E^{-1}	1.10 E^{-1}	1.29 E^{-1}	1.20 E^{-1}	1.16 E^{-1}
RG_396.1kg_512	0.57	0.87	1.06	1.24 E^{-1}	1.24 E^{-1}	1.08 E^{-1}	1.22 E^{-1}	1.17 E^{-1}	1.14 E^{-1}
RG_430kg_651	0.53	1.00	1.00	1.37 E^{-1}	1.33 E^{-1}	1.35 E^{-1}	1.46 E^{-1}	1.47 E^{-1}	1.44 E^{-1}
2A_401_30LC	0.69	1.21	0.89	3.57 E^{-2}	3.46 E^{-2}	4.27 E^{-2}	3.36 E^{-2}	3.65 E^{-2}	3.87 E^{-2}
3A_511_30LC	0.70	1.39	0.90	3.12 E^{-2}	3.38 E^{-2}	4.51 E^{-2}	2.97 E^{-2}	3.20 E^{-2}	3.37 E^{-2}
4A_622_30LC	0.66	1.57	0.78	4.16 E^{-2}	3.95 E^{-2}	6.36 E^{-2}	3.97 E^{-2}	5.18 E^{-2}	4.95 E^{-2}
5G_628_30LC	0.68	1.47	0.77	3.37 E^{-2}	3.38 E^{-2}	4.97 E^{-2}	3.32 E^{-2}	4.32 E^{-2}	4.28 E^{-2}
7G_698_30LC	0.65	1.56	0.83	4.27 E^{-2}	4.49 E^{-2}	6.83 E^{-2}	4.19 E^{-2}	4.89 E^{-2}	5.24 E^{-2}
MF_495kg_651	0.46	1.08	0.95	1.93 E^{-1}	2.10 E^{-1}	2.17 E^{-1}	2.16 E^{-1}	2.21 E^{-1}	2.33 E^{-1}
MF_502kg_651	0.45	1.12	0.94	2.00 E^{-1}	2.02 E^{-1}	2.26 E^{-1}	2.13 E^{-1}	2.28 E^{-1}	2.27 E^{-1}
MF_512kg_651	0.44	1.07	0.96	2.38 E^{-1}	2.40 E^{-1}	2.55 E^{-1}	2.50 E^{-1}	2.59 E^{-1}	2.60 E^{-1}
MF_522kg_542	0.43	0.94	1.03	2.50 E^{-1}	2.42 E^{-1}	2.30 E^{-1}	2.59 E^{-1}	2.56 E^{-1}	2.50 E^{-1}
MF_544kg_651	0.41	1.08	0.97	3.64 E^{-1}	3.43 E^{-1}	3.83 E^{-1}	3.70 E^{-1}	3.92 E^{-1}	3.73 E^{-1}

Table 2: Mechanical properties (Young's and shear moduli).

Supporting Information for Wautier, A., C. Geindreau, and F. Flin (2015), Linking snow microstructure to its macroscopic elastic stiffness tensor: A numerical homogenization method and its application to 3-D images from X-ray tomography, *Geophys Res. Lett., 42,* doi:10.1002/2015GL065227

Sample name	Porosity	ν_{12}	ν_{13}	ν_{23}	ν_{21}	ν_{31}	ν_{32}
PP_102kg_512	0.89	1.38 E^{-1}	1.46 E^{-1}	1.29 E^{-1}	1.53 E^{-1}	1.33 E^{-1}	1.05 E^{-1}
PP_113kg_600	0.88	1.57 E^{-1}	1.51 E^{-1}	1.42 E^{-1}	1.63 E^{-1}	1.32 E^{-1}	1.18 E^{-1}
PP_123kg_600	0.87	1.13 E^{-1}	1.17 E^{-1}	1.56 E^{-1}	1.46 E^{-1}	1.33 E^{-1}	1.37 E^{-1}
DF_157kg_512	0.83	1.46 E^{-1}	1.95 E^{-1}	1.59 E^{-1}	1.60 E^{-1}	1.15 E^{-1}	8.57 E^{-2}
DF_147kg_512	0.84	1.60 E^{-1}	1.55 E^{-1}	1.53 E^{-1}	1.41 E^{-1}	1.50 E^{-1}	1.68 E^{-1}
RG_172kg_600	0.81	1.70 E^{-1}	1.20 E^{-1}	1.29 E^{-1}	1.63 E^{-1}	1.02 E^{-1}	1.15 E^{-1}
RG_192kg_600	0.79	1.73 E^{-1}	1.33 E^{-1}	1.78 E^{-1}	1.78 E^{-1}	1.33 E^{-1}	1.73 E^{-1}
RG_198kg_600	0.78	1.63 E^{-1}	1.58 E^{-1}	1.82 E^{-1}	1.54 E^{-1}	1.24 E^{-1}	1.52 E^{-1}
RG_256kg_512	0.72	1.61 E^{-1}	1.78 E^{-1}	1.42 E^{-1}	1.41 E^{-1}	1.50 E^{-1}	1.36 E^{-1}
RG_280kg_512	0.69	2.06 E^{-1}	1.95 E^{-1}	1.83 E^{-1}	1.90 E^{-1}	1.08 E^{-1}	1.10 E^{-1}
1A_350_30LC	0.70	1.34 E^{-1}	1.24 E^{-1}	1.39 E^{-1}	1.46 E^{-1}	1.56 E^{-1}	1.59 E^{-1}
0A_261_30LC	0.69	1.69 E^{-1}	1.59 E^{-1}	1.70 E^{-1}	1.50 E^{-1}	1.33 E^{-1}	1.60 E^{-1}
RG_315kg_512	0.66	1.81 E^{-1}	1.87 E^{-1}	1.47 E^{-1}	1.40 E^{-1}	1.82 E^{-1}	1.86 E^{-1}
RG_1600	0.64	1.66 E^{-1}	1.72 E^{-1}	1.78 E^{-1}	1.62 E^{-1}	1.60 E^{-1}	1.69 E^{-1}
RG_1600sup800	0.63	1.65 E^{-1}	1.75 E^{-1}	1.89 E^{-1}	1.83 E^{-1}	1.59 E^{-1}	1.55 E^{-1}
RG_354kg_512	0.61	1.71 E^{-1}	1.83 E^{-1}	1.90 E^{-1}	1.80 E^{-1}	1.77 E^{-1}	1.75 E^{-1}
RG_359kg_600	0.61	1.68 E^{-1}	1.97 E^{-1}	1.76 E^{-1}	1.66 E^{-1}	1.81 E^{-1}	1.63 E^{-1}
RG_378kg_512	0.59	1.84 E^{-1}	2.03 E^{-1}	1.88 E^{-1}	1.85 E^{-1}	1.48 E^{-1}	1.37 E^{-1}
RG_396kg_512	0.57	1.90 E^{-1}	1.62 E^{-1}	1.81 E^{-1}	1.79 E^{-1}	1.44 E^{-1}	1.70 E^{-1}
RG_396.1kg_512	0.57	1.53 E^{-1}	1.83 E^{-1}	1.79 E^{-1}	1.54 E^{-1}	1.60 E^{-1}	1.56 E^{-1}
RG_430kg_651	0.53	1.93 E^{-1}	1.94 E^{-1}	1.90 E^{-1}	1.88 E^{-1}	1.91 E^{-1}	1.92 E^{-1}
2A_401_30LC	0.69	1.61 E^{-1}	1.29 E^{-1}	1.34 E^{-1}	1.55 E^{-1}	1.54 E^{-1}	1.66 E^{-1}
3A_511_30LC	0.70	1.36 E^{-1}	1.15 E^{-1}	1.05 E^{-1}	1.47 E^{-1}	1.67 E^{-1}	1.41 E^{-1}
4A_622_30LC	0.66	1.50 E^{-1}	1.35 E^{-1}	1.12 E^{-1}	1.42 E^{-1}	2.06 E^{-1}	1.81 E^{-1}
5G_628_30LC	0.68	1.47 E^{-1}	1.26 E^{-1}	1.25 E^{-1}	1.47 E^{-1}	1.85 E^{-1}	1.84 E^{-1}
7G_698_30LC	0.65	1.42 E^{-1}	1.18 E^{-1}	1.07 E^{-1}	1.49 E^{-1}	1.89 E^{-1}	1.63 E^{-1}
MF_495kg_651	0.46	1.94 E^{-1}	1.84 E^{-1}	2.14 E^{-1}	2.11 E^{-1}	2.06 E^{-1}	2.21 E^{-1}
MF_502kg_651	0.45	2.01 E^{-1}	2.00 E^{-1}	1.91 E^{-1}	2.02 E^{-1}	2.25 E^{-1}	2.13 E^{-1}
MF_512kg_651	0.44	2.01 E^{-1}	2.02 E^{-1}	2.04 E^{-1}	2.03 E^{-1}	2.17 E^{-1}	2.17 E^{-1}
MF_522kg_542	0.43	2.15 E^{-1}	2.14 E^{-1}	2.16 E^{-1}	2.08 E^{-1}	1.97 E^{-1}	2.06 E^{-1}
MF_544kg_651	0.41	2.31 E^{-1}	2.24 E^{-1}	2.08 E^{-1}	2.17 E^{-1}	2.36 E^{-1}	2.33 E^{-1}

Table 3: Mechanical properties (Poisson's ratios).

2 Temporal series

In this section, the 3D microtomographic images corresponding to the three temporal series considered in the titled paper are shown:

- The 8 images used in the study of isothermal metamorphism are visible in Figure 1;
- The 7 images used in the study of temperature gradient metamorphism are visible in Figure 2;
- The 5 images used in the study of wet snow metamorphism are visible in Figure 3.

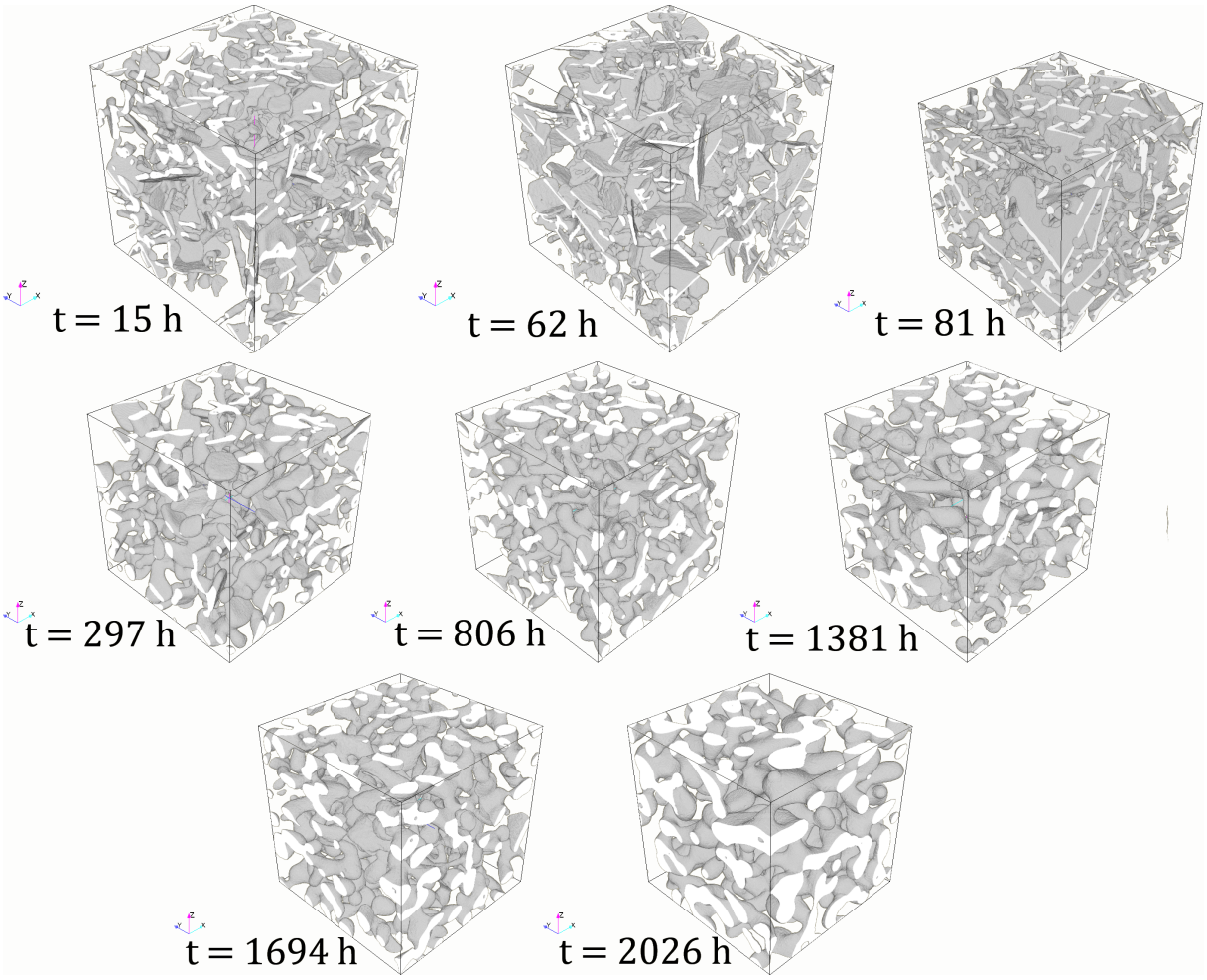

Figure 1: Microstructure evolution corresponding to the experiment of isothermal metamorphism presented in section 5.1 of the related paper. Further information can be found in the work of *Flin et al.* (2004).

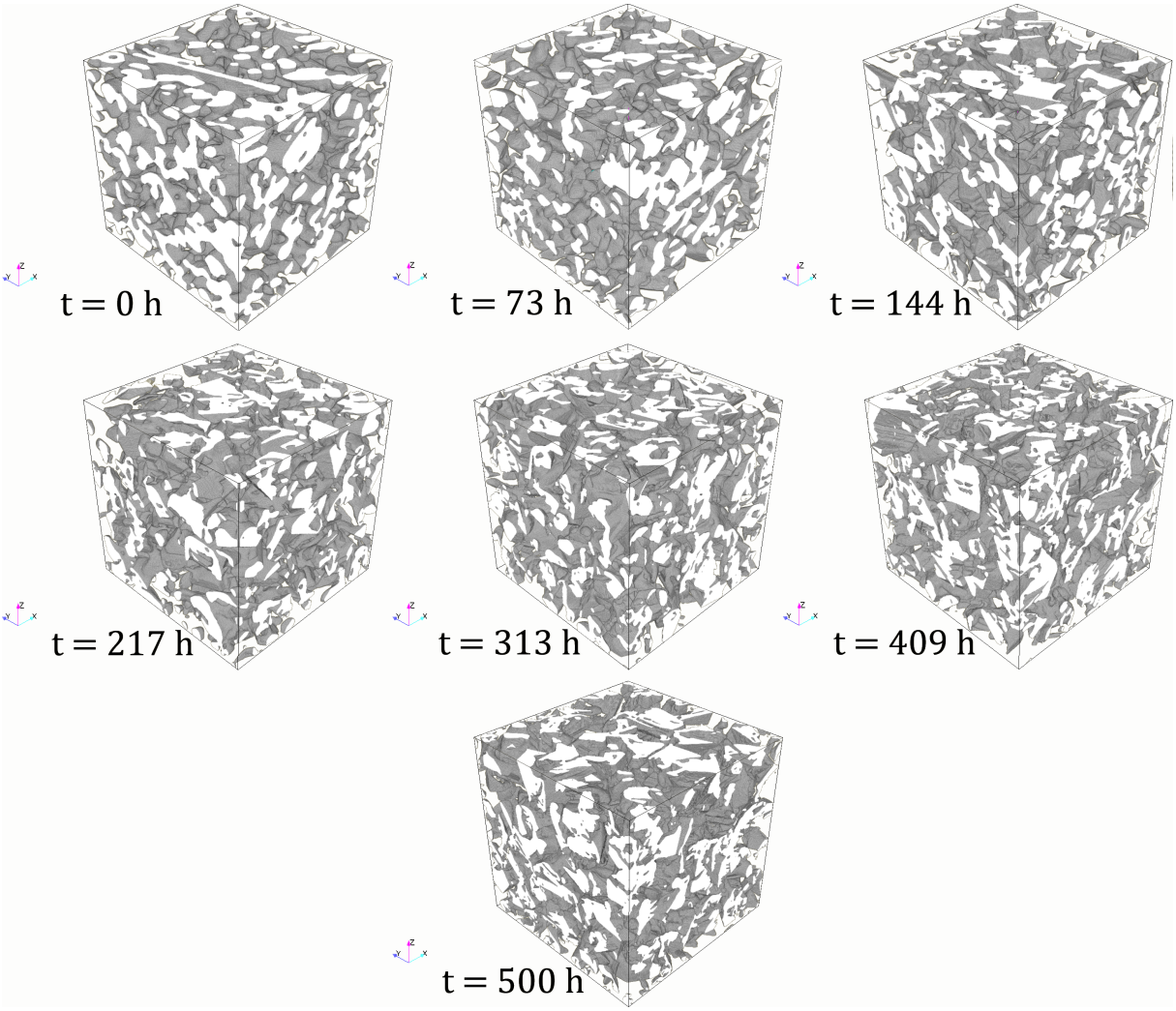

Figure 2: Microstructure evolution corresponding to the experiment of temperature gradient metamorphism presented in section 5.2 of the related paper. Further information can be found in the work of *Calonne et al.* (2014).

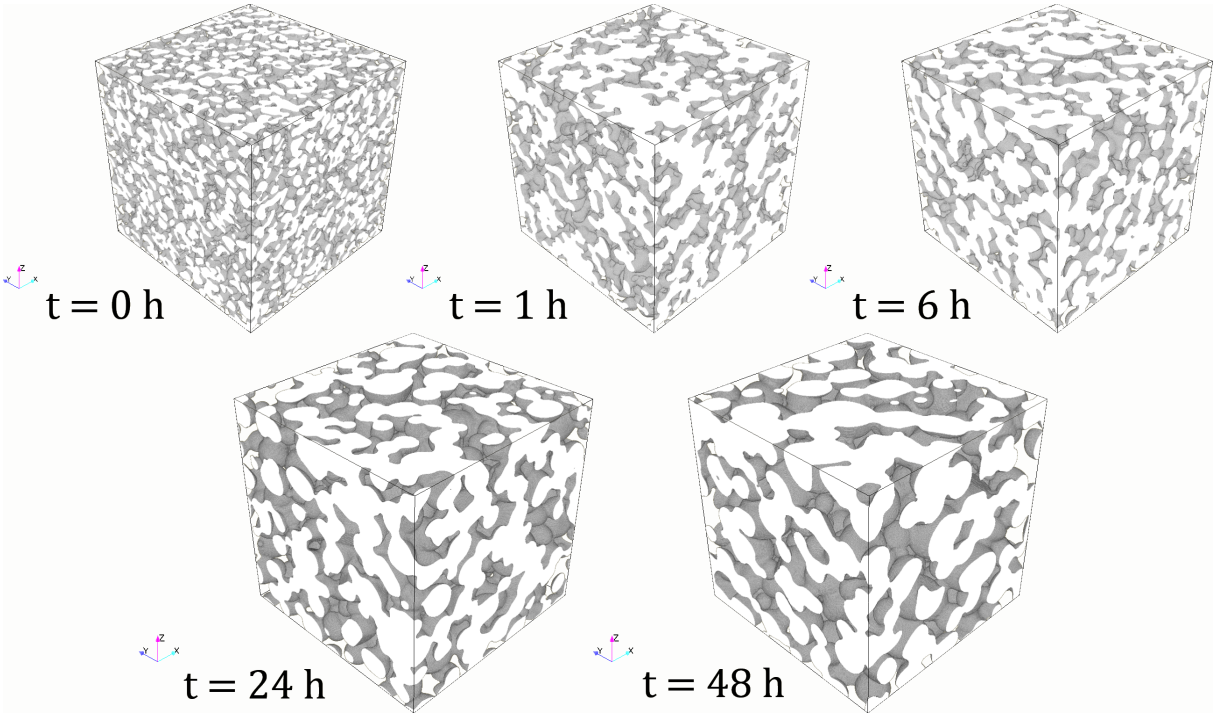

Figure 3: Microstructure evolution corresponding to the experiment of wet snow metamorphism presented in section 5.3 of the related paper. Further information can be found in the work of *Flin et al.* (2011).

References

Calonne, N., C. Geindreau, F. Flin, S. Morin, B. Lesaffre, S. Rolland du Roscoat, and P. Charrier (2012), 3-Dimage-based numerical computations of snow permeability: links to specific surface area, density, and microstructural anisotropy, *The Cryosphere*, *6*(5), 939–951, doi:10.5194/tc-6-939-2012.

Calonne, N., F. Flin, C. Geindreau, B. Lesaffre, and S. Rolland du Roscoat (2014), Study of a temperature gradient metamorphism of snow from 3-D images: time evolution of microstructures, physical properties and their associated anisotropy, *The Cryosphere*, *8*(6), 2255–2274, doi:10.5194/tc-8-2255-2014.

Fierz, C., R. L. Armstrong, Y. Durand, P. Etchevers, E. Greene, D. M. McClung, K. Nishimura, P. K. Satyawali, and S. A. Sokratov (2009), *The international classification for seasonal snow on the ground*, UNESCO/IHP, Paris.

Flin, F., J.-B. Brzoska, B. Lesaffre, C. Coléou, and R. A. Pieritz (2004), Three-dimensional geometric measurements of snow microstructural evolution under isothermal conditions, *Annals of Glaciology*, *38*(1), 39–44, doi:10.3189/172756404781814942.

Flin, F., B. Lesaffre, A. Dufour, L. Gillibert, A. Hasan, S. Rolland du Roscoat, S. Cabanes, and P. Puglièse (2011), On the computations of specific surface area and specific grain contact area from Snow 3D images, in *Physics and Chemistry of Ice*, edited by Y. Furukawa, pp. 321–328, Hokkaido University Press, Sapporo, Japan, Proceedings of the 12th International Conference on the Physics and Chemistry of Ice held at Sapporo, Japan on 5-10 September 2010.

Löwe, H., F. Riche, and M. Schneebeli (2013), A general treatment of snow microstructure exemplified by an improved relation for thermal conductivity, *The Cryosphere*, *7*(5), 1473–1480, doi:10.5194/tc-7-1473-2013.